Transient telomerase inhibition alters cell cycle kinetics

Connor AH Thompson 1, Alice YM Gu 1, Sunny Y Yang 1, Veena Mathew 2, Helen B Fleisig 1, and Judy MY Wong 1.

1 Faculty of Pharmaceutical Sciences, University of British Columbia
2 Terry Fox Laboratory, British Columbia Cancer Research Centre, BC Cancer Agency.

Running Title: Telomerase inhibition alters cell cycle kinetics

Keywords: telomerase, telomere, telomere loop, cell cycle, imetelstat

Financial support for this work was provided by Research Investment Funds from the Faculty of Pharmaceutical Sciences at UBC.

Corresponding author:
Judy Wong
University of British Columbia
2405 Westbrook Mall
Vancouver, BC
Canada V6T 1Z3

Ph 604-827-3314
FAX 604-822-3035
judy.wong@ubc.ca

Classification: Biological Sciences - Cell Biology

Conflict of interest:
The authors declare no conflict of interest.

Imetelstat provided by Geron Corporation.

Abstract: 250 words
Significance statement: 111 words
Main text: 4636 words
Figures: 6

ABSTRACT

Telomerase is the ribonucleoprotein reverse transcriptase that catalyzes the synthesis of telomeres at the ends of linear human chromosomes and contributes to proper chromosomal capping function. Formation of the telomere-loop (T-loop), an obligate step before cell division can proceed, requires the generation of a 3'-overhang on the G-rich strand of telomeric DNA via telomerase or C-strand specific nucleases. Here, we discover telomerase activity is critical for efficient cell cycle progression using transient chemical inhibition by the telomerase inhibitor imetelstat. Telomerase inhibition caused changes in cell cycle kinetics and increased the proportion of cells in G2 phase, suggesting delayed clearance through this checkpoint. Investigating the possible contribution of unstructured telomere ends to these cell cycle distribution changes, we observed that imetelstat treatment induced γH2AX DNA damage foci in a subset of telomerase-positive cells but not telomerase-negative primary human fibroblasts. Chromatin-immunoprecipitation with γH2AX antibodies demonstrated imetelstat treatment-dependent enrichment of this DNA damage marker at telomeres. Notably, the effects of telomerase inhibition on cell cycle profile alterations were abrogated by pharmacological inhibition of the DNA-damage-repair transducer ATM. Additionally, imetelstat potentiation of etoposide, a DNA-damaging drug that acts preferentially during S/G2 phases of the cell cycle, also depended on functional ATM signaling. Our results suggest that telomerase inhibition delays the kinetics of T-loop formation in telomerase-positive cancer cells, resulting in the engagement of an ATM-dependent DNA-damage signal

71 that prevents cell cycle progression. This demonstrates for the first time that
72 telomerase activity directly modulates the progression of the cell cycle through
73 facilitation of T-loop formation.
74
75
76
77
78
79
80
81
82
83
84
85
86
87
88
89
90
91
92
93

SIGNIFICANCE STATEMENT

By forming higher-order capping structures, telomeres protect the ends of linear chromosomes from inappropriate recognition as DNA damage. An important component of this process is the formation of a 3'-overhang on the G-rich strand. This can be accomplished by the action of C-strand-specific nucleases or via telomere repeat synthesis by the telomere-maintenance enzyme telomerase. Here, using a chemical telomerase inhibitor, we demonstrate that telomerase facilitates the kinetics of telomere cap formation and passage through G2 phase. Inhibition of telomerase activity results in a prolonged ATM-dependent DNA-damage signal that alters cell cycle kinetics. Our data provide the biological rationale for exploring clinical telomerase inhibition strategies that leverage possible telomere-length-independent mechanisms of activity.

INTRODUCTION

Telomeres are nucleoprotein structures present at the ends of eukaryotic linear chromosomes. Telomeres differentiate the ends of chromosomes from random DNA breaks through the formation of capping structures called telomere loops (T-loops). These higher-order capping structures are essential for proper telomere function and cell cycle progression. In mammals, telomeres are composed of repeated sequences of $(TTAGGG)_n$ nucleotides, the complementary DNA strands, and associated proteins (1). Telomeres prevent the loss of coding DNA sequence by buffering the lagging strand gap left by the removal of RNA primers, thereby solving the “end replication problem”. Telomeric DNA loss also results from T-loop resolution, an obligatory step to provide access for DNA replication machinery. Together, these processes contribute to the loss of 50-100 base pairs of 3’ terminal telomeric DNA with each replication cycle (2). This telomere attrition forms the basis of the Hayflick Limit and restricts the number of times a cell lineage may proliferate (3).

Telomeres are maintained by the ribonucleoprotein telomerase. Telomerase has two main components: the catalytic telomerase reverse transcriptase (TERT) and the template telomerase RNA (TER). TERT catalyzes the synthesis of the hexanucleotide repeats by reverse transcribing the RNA template sequences encoded in TER (4-7). This telomerase-mediated telomere elongation promotes immortal growth by decoupling the cell division limit from telomere length attrition.

TERT expression is normally repressed or only transiently activated in somatic human cells, but telomerase activation and over-expression is detected in 85-90% of human cancers (8,9). These differences make telomerase inhibition an attractive therapeutic target (1,5-7,11,12,19). One current strategy for telomerase inhibition is the drug imetelstat (GRN163L), a synthetic, lipid-conjugated, 13-mer oligonucleotide N3' P5' thiophosphoramidate complementary to the template of the TER component of telomerase (4,10,12,16-18,20). As a competitive antagonist, imetelstat blocks the normal association of TER with chromosomal ends (substrates), efficiently inhibiting *de novo* telomeric repeat synthesis.

During the DNA-synthesis phase of the cell cycle, the activities of multiple RecQ helicases, exonucleases, homologous recombination pathway effectors, and histone methylation enzymes are coordinated to allow DNA polymerase and telomerase (when expressed) to copy through T-loops and then restore the heterochromatin state of newly replicated telomeres (8,10-14). Defects in telomere-associated proteins involved in T-loop formation, such as helicases (BLM, RTEL1), nucleases (Apollo), or telomere factors (TRF1, TRF2), have been connected to uncapped telomeres, which can lead to cell cycle arrest and ultimately, cell senescence or apoptosis (10,12,15-18,22). Additionally, the correct rebuilding of chromosomal-end structures prior to cell division has been shown to involve the Ataxia Telangiectasia Mutated (ATM) signal transduction pathway (5-7,20,21). Activation of ATM and its associated PIKK-family member,

the ATM-related (ATR) kinase, is concurrent with T-loop resolution and the resulting chromosome termini exposure (8,9,11,12,19).

Specifically, T-loop formation requires the creation of telomeric G-rich overhangs that invade the double-stranded telomeric DNA region and form displacement loops (1,10). In primary cells, telomerase is inactive and the generation of G-rich overhangs and T-loops is dependent upon C-strand-specific nuclease activity (1,10,12,15-18). In cancer cells, telomerase expression provides another avenue for the de novo synthesis of G-rich telomeric DNA repeats, in addition to nuclease activity (1,10,12,15-18). However, this role of active telomerase in the kinetics of T-loop formation has been inferred from its ability to synthesize G-rich telomeric repeats but has not been demonstrated experimentally.

Here, we used imetelstat-induced chemical inhibition of telomerase activity to explore the role of *de novo* telomeric DNA repeat synthesis in the kinetics of T-loop formation. Since chemical inhibition is transient, we were able to study the effects of telomerase activity on structure without significant shortening of telomere length. Transient chemical inhibition also allows the immediate observation of treatment effects, thus reducing the impact of compensatory mechanisms that may confound observations.

RESULTS

Telomerase inhibition increases the proportion of cells in G2/M phases of the cell cycle

184 During normal DNA replication, DNA-damage-response (DDR) signaling is
185 found transiently in late S/G2 phases at unstructured, open chromosome ends.
186 These signals have been detected in the forms of ATM-MRN and ATR-ATRIP
187 complexes (5,8,21,25,26). In order for cells to properly divide, DDR signals must
188 first be cleared by the reformation of T-loops. To understand how telomerase
189 may affect the kinetics of T-loop formation, we measured the effects of
190 imetelstat-induced telomerase inhibition on cell cycle progression.
191 Cells were treated with 10 μM inhibitory doses of imetelstat (5) or its
192 mismatch oligo control (MM) (27) for 24 h before harvesting and staining with
193 propidium iodide (PI) for cell cycle profiling using fluorescence-activated cell
194 sorting (FACS). In telomerase-positive mammary adenocarcinoma (MCF-7 and
195 MDA-MB 231) and colorectal carcinoma (HT29 and LS180) cells, a significant
196 increase in cell populations with 4N DNA content following imetelstat but not MM
197 treatment was observed (Fig. 1 a-d). In contrast, the cell cycle profiles of
198 telomerase-negative transformed cells (VA-13), which maintain telomeres via the
199 alternative lengthening of telomere (ALT) mechanism (28), and primary human
200 foreskin fibroblasts (BJ) were unaltered by both imetelstat and MM (Fig. 1 e-f).
201 The increased 4N cell population was likely due to a delay in exit from G2
202 phase rather than a cell cycle arrest, as previous studies have reported normal
203 cell growth following the removal of imetelstat (5). This suggests that treated cells
204 can return to normal cycling after the removal of drugs. To confirm the delayed
205 exit from G2 phase, we further investigated the proliferative capacity of cells after
206 imetelstat treatment. We used the IncuCyte Zoom live cell imaging system and

red fluorescent NucLight-tagged MDA-MB 231 cells to measure the effects of continuous imetelstat treatment on cell proliferation over 7 days. Consistent with a small but accumulative growth disadvantage conferred by delayed clearance from G2 phase, we observed lower nuclear counts in cells exposed to 10 μM imetelstat compared to untreated cells (Supplementary Fig. 1 a). A lower dose of imetelstat (2 μM) resulted in an intermediate growth effect that is in agreement with reduced inhibition of cellular telomerase activity (Supplementary Fig. 2, left panel).

In order to measure growth in MCF-7 cells, we used the same treatment regimen and measured absolute cell counts by Coulter counting. Similar to before, a subtle growth defect was observed in MCF-7 cells treated with 10 μM imetelstat (Supplementary Fig. 1 b). In contrast, imetelstat had no apparent effect on cellular proliferation of telomerase-negative VA-13 cells (Supplementary Fig. 1 c). Telomerase activity in MDA-MB 231, MCF-7, and HT29 cells was effectively inhibited by imetelstat in a dose-dependent manner, as confirmed by telomeric repeat amplification protocol (TRAP) assays (Supplementary Fig. 2). These results are consistent with a subtle imetelstat-induced defect in cell growth that is revealed under longer-term incubation conditions. Together, our data suggest that transient telomerase inhibition causes changes in cell cycle kinetics that result in a growth disadvantage.

ATM inhibition abolishes the increase in 4N DNA cells caused by imetelstat treatment

As ATM activation is concurrent with the resolution and rebuilding of telomere structures, we next examined whether the effects of imetelstat on cell cycle progression depend upon active ATM signaling. We applied pharmacological inhibitor order-of-addition treatment regimens using imetelstat (Im) and the specific ATM inhibitor KU55933 (Ku). The treatment conditions tested include: single drug treatments of imetelstat (Im|Im) or KU55933 (Ku|Ku) for 48 h; combinatorial treatment of imetelstat for 24 h then both imetelstat and KU55933 for another 24 h (Im|Im + Ku); and combinational treatment of KU55933 for 24 h then both imetelstat and KU55933 for another 24 h (Ku|Im + Ku) (Fig. 2 a).

Consistent with Figure 1 a, imetelstat (Im|Im) treatment in MCF-7 cells increased the population of cells with 4N DNA content relative to the population distribution in untreated cells (Fig. 2 b). Notably, this effect on cell cycle progression was abrogated by KU55933 pretreatment (Ku|Im + Ku) but not by treatment with KU55933 after imetelstat exposure (Im|Im + Ku). Treatment with ATM inhibitor alone (Ku|Ku) resulted in a reduction in the cell population with 4N DNA content, but this reduction was not statistically significant in our data analysis.

Treatment-induced cellular toxicities can also affect cell cycle profiles. To differentiate this possibility from phase-specific cell cycle regulation, we analyzed sub-G1 populations by FACS as a functional readout of cell death at the time of DNA content analysis. The proportions of sub-G1 cell populations were not significantly affected by single imetelstat (Im|Im) and KU55933 (Ku|Ku) treatments, or by any treatment combinations, indicating that these changes in

cell cycle profiles were unlikely to be caused by increased rates of cell death (Fig. 2 c).

Additionally, we assessed whether KU55933 interfered with the efficiency of imetelstat-induced telomerase inhibition by measuring telomerase activity with TRAP. Cells pre-treated with KU55933 (Ku|Im + Ku) also showed no telomerase activity in the presence of imetelstat (Supplementary Fig. 3), confirming that ATM inhibition did not affect imetelstat's ability to completely inhibit telomerase actions. Together, these results imply that cell cycle alterations caused by imetelstat-induced telomerase inhibition are dependent on functional ATM signaling.

Imetelstat treatment induces telomere-specific DNA damage foci during the G2 phase of telomerase-positive cells

In the absence of proper T-loop formation, uncapped telomeres are recognized as DNA damage and accumulate DNA damage foci. The formation of these damage foci is primarily mediated through the actions of ATM (26). To confirm telomerase is involved in the normal kinetics of T-loop formation, we examined the delayed clearance of ATM-induced DDR signals following imetelstat treatment. Immunocytochemistry and confocal microscopy were used to visualize the DDR marker γH2AX (Ser139), a standard marker of uncapped or dysfunctional telomeres (1,20,21,25,26).

Imetelstat treatment over 24 h increased the number of cells with γH2AX DDR foci in a subset of telomerase-positive MCF-7 and HT29 cells (Fig. 3 a-d)

but not telomerase-negative primary human BJ fibroblasts (Fig. 3 e-f). In parallel, the mismatch oligo control had no significant effect on γH2AX DDR foci accumulation. The observed increase in foci was not due to increased non-specific background labeling in imetelstat-treated cells as illustrated by the secondary antibody-alone controls (Supplementary Fig. 4).

To confirm the telomeric origin of imetelstat-induced γH2AX DDR foci, we performed chromatin-immunoprecipitation using anti- γH2AX antibody. In agreement with our immunocytochemistry observations, we confirmed increased γH2AX ChIP signals following 24h imetelstat and etoposide treatments, but not after treatments with the mismatch oligo, or vehicle control (Fig. 3 g-i). Quantitative PCR measurements of γH2AX ChIP signals showed enrichment of telomeric sequence following both imetelstat and etoposide treatments (Fig. 3 g). In contrast, γH2AX signal enrichment at Alu-repeat sequence was only observed with etoposide treatments (Fig. 3 h). When γH2AX signal enrichment at telomere was normalized to the signals measured with the Alu-repeat reference, the imetelstat group significantly different from the other three treatment groups, suggesting that imetelstat induced the formation of telomere-specific γH2AX loci (Fig. 3 i). This accumulation of γH2AX DDR foci at telomeres following imetelstat treatment is consistent with an increase in uncapped telomeres caused by the absence or inhibition of telomerase activity.

In order to assess the distribution of γH2AX DDR foci-positive cell populations and their corresponding cell cycle phase, using immunohistochemistry, we co-labeled imetelstat-treated MCF-7 and HT29 cells

with DDR and cell cycle phase markers. Since γH2AX DDR foci-positive cells co-labeled with cytoplasmic cyclin B1, a marker of late S/G2 phases (Fig. 4 a-d), but not phospho-histone H3 (H3P), an M phase marker in MCF-7 cells (Fig. 4 e-f), the γH2AX DDR foci-positive cells were concluded to be residing in the S/G2 phases.

Consistent with the immunocytochemistry data, FACS measurements showed the proportion of MCF-7 cells that were both cyclin B1-positive and contained 4N DNA content increased with imetelstat treatment, relative to no drug treatment and/or mismatch oligo controls (Fig. 4 g-h). Considering that the magnitude of this increase was small, a delayed clearance from, rather than a complete arrest at, G2 phase was more likely. Overall, our data indicate that imetelstat-induced telomerase inhibition correlates with an accumulation of DDR marker γH2AX and a delayed clearance of the telomere checkpoint at G2 phase of the cell cycle.

Transient telomerase inhibition-induced DDR foci formation depends upon active ATM signaling

Imetelstat was observed to delay G2 checkpoint clearance in an ATM-activity dependent manner. To connect the role of ATM in G2 checkpoint regulation with imetelstat-dependent γH2AX DDR foci formation, we again used our order-of-addition experimental scheme coupled with immunofluorescent detection of DDR signals. MCF-7 cells were treated with KU55933 and imetelstat for 48 h, either alone or in different combinations, and γH2AX DDR foci were

quantified. As in our previous experiments, imetelstat treatment (Im|Im) resulted in an increase in γH2AX DDR foci relative to the untreated (NT) negative control (Fig. 5 a-b). Also as expected, we observed that treatment with KU55933 alone (Ku|Ku) or before imetelstat addition (Ku|Im + Ku) abolished γH2AX DDR foci formation. Interestingly, treatment with KU55933 after 24 h incubation with imetelstat (Im|Im + Ku) only showed a slight, but not statistically significant, reduction in γH2AX DDR foci formation. It is conceivable that blocking the activity of ATM prevents the phosphorylation and propagation of new γH2AX foci but does not remove the phosphorylated proteins that have already formed (Fig. 5 a-b).

To provide further insight into the fate of imetelstat-treated cells that escape G2-stalling, we labeled cells from different treatment groups for phospho-histone H3P and quantified the proportion of cells progressing to M phase (Fig. 5 a, c). When no drug treatment was administered, ~5% of MCF-7 cells were H3P-positive. Treatment with imetelstat alone (Im|Im) decreased the proportion of cells in M phase, consistent with a stall at the G2 checkpoint due to persistent DDR signaling. In contrast, cells treated with imetelstat and then KU55933 (Im|Im + Ku) showed an increase in the proportion of cells in M phase, suggesting that continuous ATM signaling is essential for the G2 stall caused by imetelstat-induced DDR signaling. Blocking ATM signaling following transient telomerase inhibition likely released MCF-7 cells from the G2 checkpoint and allowed progression to the next phase of the cell cycle. This release of previously stalled cells manifested as an increase in cells entering M phase.

Similar to continuous imetelstat treatment, treatment with KU55933 alone (Ku|Ku) or prior to imetelstat addition (Ku|Im + Ku) reduced the number of M-phase cells, suggesting that the order of ATM and telomerase inhibition is important. Consistent with the relative decrease in 4N DNA cell populations observed in our earlier FACS experiments (Fig. 2 b), ATM inhibition may induce faster passage through G2/M phases using multiple parallel mechanisms (see discussion) such that the effects of telomerase inhibition are masked. Our data demonstrate that ATM inhibition before imetelstat treatment removed the effects of telomerase-inhibition–induced G2 stalling, confirming that functional ATM activity is essential for the telomere checkpoint.

Imetelstat potentiation of etoposide cytotoxicity depends upon active ATM signaling

Previously, we observed that imetelstat potentiated the cytotoxicity of S/G2-specific DNA-damaging agents, including the topoisomerase inhibitors etoposide and irinotecan (5). Addition of ATM inhibitor KU55933 following 24 h of imetelstat treatment (Im|Im + Ku) further increased the cytotoxicity of etoposide. However, the cytotoxic effects from inhibition of ATM signaling before imetelstat treatment (Ku|Im + Ku) were not tested in this previous study. To clarify the role of ATM signaling in imetelstat-induced potentiation of etoposide cytotoxicity, we again performed order-of-addition treatment experiments using the colony forming unit assay (5-7,12,16). MCF-7 cells were pre-treated for 24 h with imetelstat or KU55933 before the addition of etoposide with continued inhibitor

368 treatment or in combination with both imetelstat and KU55933 for 24 h. After 48 h
369 of treatment, cells were harvested and set in soft agar medium to recover for 2
370 weeks (Fig. 6 a).

371 In agreement with previous results, imetelstat (Im|Im) or KU55933 (Ku|Ku)
372 treatment alone significantly potentiated etoposide cytotoxicity in MCF-7 cells
373 (Fig. 6 b-c) (5,10-14,29). ATM inhibition consistently resulted in greater
374 potentiation of etoposide cytotoxicity than imetelstat-induced telomerase
375 inhibition alone. This observation was attributed to the broader role of ATM in
376 signal transduction regulation of cellular responses to double-strand DNA
377 damage (30), in addition to its role in telomere maintenance and structural
378 homeostasis.

379 Consistent with our previous data, an additive effect on etoposide
380 cytotoxicity was observed when the cells were treated with both inhibitors in
381 combination following imetelstat pre-treatment (Im|Im + Ku). In contrast, the
382 additive effect was lost when cells were pre-treated with KU55933 before
383 imetelstat and KU55933 addition (Ku|Im +Ku). These observations suggest that
384 functional ATM-dependent DDR signaling is required for the potentiation of
385 etoposide cytotoxicity by telomerase inhibition.

386 Notably, the rank order of treatment conditions leading to increased
387 sensitivities towards etoposide mirrors the rank order of treatment conditions
388 leading to increased DDR foci accumulation observed in our previous FACS
389 experiments. The most cytotoxic treatment condition (Im|Im + Ku) was also
390 observed to increase the proportion of cells in M phase in our previous ICC

391 experiments. Based on these observations, we reasoned that the increased
392 cytotoxicity might be linked to increased mitotic errors caused by the premature
393 release of chromosomes with unstructured telomeres from the G2 checkpoint.
394 Consistent with improperly capped telomeres proceeding to mitosis, following
395 treatment (Im|Im + Ku), we observed an increase in micronuclei formation that
396 indicated mitotic defects and increased genomic instability (Fig. 6 d-e). This
397 increase in the number of cells with mitotic defects acts as an additional cytotoxic
398 mechanism in etoposide-treated MCF-7 cells.
399

400 **DISCUSSION**

401 ***TERT addiction manifests as a kinetic advantage in cell cycle progression***

402 The role of telomerase in telomeric chromatin formation is inferred through
403 its *de novo* telomere synthesis function but has never been directly
404 demonstrated. Our data suggest that telomerase improves the kinetics of G-rich
405 overhang formation and thus, facilitates efficient higher-order telomeric chromatin
406 formation and clearance from the G2 checkpoint.

407 In telomerase-positive cells, imetelstat blocks the access of reverse
408 transcriptase to its telomeric DNA substrate, thereby preventing *de novo*
409 synthesis of G-rich telomere repeats (10,12,15-18,20,31). Consequently, ATM-
410 mediated DDR signals at unstructured telomeres take longer to resolve. This
411 results in delayed passage through cell cycle checkpoints and a temporary
412 accumulation of cells in G2 phase.

The lack of telomerase action stalls but does not entirely arrest cells at G2 phase because G-rich overhangs for T-loop formation can still be produced, albeit with reduced efficiency, through the actions of multiple nucleases (11,12,16,19,32). In the absence of G-strand synthesis, Exo1 provides more substantial resection for T-loop formation. However, nuclease recruitment and processing may have slower kinetics than telomere repeat synthesis (10,15). Therefore, the inhibition of telomerase will delay, but not stop, the progression of the cell cycle.

The observation that telomerase improves the kinetics of T-loop formation is consistent with previous work from our laboratory showing that overexpression of telomerase in telomerase-negative ALT cells conferred a growth advantage and faster passage through S/G2 phases of the cell cycle (20,21,30,33). This selective growth advantage may cause cancer cells to become “addicted” to telomerase activity and explain the preponderance of telomerase overexpression (>85%) for telomere maintenance over the alternate lengthening of telomere mechanism in surveyed cancers (28).

As telomerase-negative cells reform T-loops using C-strand-specific nucleases, their cell cycle progression is predicted to be unaltered by imetelstat treatment (5,7,8,15,21,25,26). This prediction is supported by the lack of significant decreases in cell growth in imetelstat-treated telomerase-negative cell lines (Supplementary Fig. 1 c). Therefore, somatic tissues with low telomerase expression are also predicted to have tolerable clinical toxicity profiles for telomerase inhibition by imetelstat (1,5-7,20).

436 ***ATM signaling is necessary for telomerase actions at the T-loop***

437 Functional ATM is required for normal elongation of telomeres by
438 telomerase in human cells (5,10-14,23,24,34). ATM inhibition prior to imetelstat
439 treatment abolishes the delay in cell cycle progression induced by telomerase
440 inhibition. This observation may be due to the inhibition of telomerase recruitment
441 to the telomere in the absence of ATM activity (22) or the inhibition of a
442 telomerase-independent ATM function that leads to changes in G2 checkpoint
443 engagement (35).

444 Notably, ATM inhibition was previously shown to accelerate passage
445 through G2 phase by the removal of inhibitory phosphorylation of C-strand-
446 specific Exo1 nuclease (31). Increased Exo1 activity leads to faster G-rich
447 overhang formation and thus, increases the kinetics of T-loop formation in the
448 absence of telomerase actions. Accordingly, accelerated G2/M progression is
449 consistent with the observed trend of reduced populations of cells with 4N DNA
450 content following KU55933 treatment (Fig. 2 b).

451 Interestingly, reversal of the order of inhibitor addition, with the addition of
452 imetelstat before ATM inhibition, resulted in increases in M-phase cell
453 populations. This suggests that the ATM-dependent telomere checkpoint was
454 quickly engaged following telomerase inhibition. Subsequent ATM inhibition
455 released previously stalled cells from G2 phase to M phase, confirming that
456 continuous ATM signaling is crucial for the maintenance of this checkpoint (36).
457 In M phase, uncapped chromosome ends resulted in abnormal cell division
458 and/or mitotic catastrophe (Fig. 6 d-e). The higher levels of micronuclei formation

459 indicate possible mitotic defects and chromosomal instability due to errors in
460 telomere processing.
461
462 ***Therapeutic implications of short-term telomerase inhibition***
463 Previous work in our laboratory demonstrated that combining telomerase
464 inhibition by imetelstat with genotoxic agents potentiated the cytotoxic effects of
465 G2-specific DNA-damaging agents such as topoisomerase inhibitors (5,11,12).
466 Data from our current study indicate that this potentiating effect is likely due to an
467 ATM-dependent DNA-damage signal induced by telomerase inhibition. The
468 sustained DDR signal at unstructured chromosome ends may act in an additive
469 manner with G2-specific DNA-damaging agents such that a greater proportion of
470 cells pass the apoptotic threshold. Our hypothesis is supported by previous
471 observations that telomerase depletion in yeast caused chronic replication stress
472 and stalled replication forks (32). In this context, topoisomerase inhibitors and
473 other drugs that cause replicative stress may synergize particularly well with
474 imetelstat.
475 The potentiation of topoisomerase inhibitors by imetelstat may also be due
476 to pharmacodynamic interactions between telomerase inhibition and
477 topoisomerase inhibition. As previously observed, proper T-loop formation may
478 involve topoisomerase activity (7). The loss of telomerase activity in combination
479 with the absence of topology relief may further damage telomere structures and
480 result in cytotoxicity responses, thus providing another mechanism by which
481 imetelstat can potentiate topoisomerase inhibitor cytotoxicity.

In order for telomeres to shorten significantly, multiple rounds of cellular replication are required. The long lag time associated with telomere shortening has been a major theoretical barrier to the utilization of telomerase inhibitors for anti-cancer chemotherapy (1). Recent clinical trials of imetelstat in myelofibrosis and thrombocythemia have cast doubt on this premise. Telomere length did not change in response to therapy and baseline telomere length was not predictive of a positive therapeutic response (8,23,37). In this context, our data provide an alternate explanation for the observed clinical effects of imetelstat: telomerase inhibition in these hematopoietic cell types may induce distortions in cell cycle kinetics without parallel observable effects on telomere-length regulation.

Telomeric-DNA-replication stress due to telomerase inhibition may be partially relieved by an increase in the dNTP (purine) pool, as suggested in previous studies (6,7,32). However, hematopoietic cancers frequently display dysregulated dNTP metabolism (10,11,13,14,38). Therefore, this model predicts that existing therapeutic agents targeting the available dNTP pools, such as mycophenolic acids, will have synergistic effects with imetelstat treatments in vulnerable hematopoietic cell types.

We observed that transient telomerase inhibition by imetelstat altered the kinetics of T-loop formation through the engagement of the G2 checkpoint. Imetelstat also sensitized telomerase-positive cells to G2-specific DNA-damaging agents through delayed resolution of an ATM-dependent DNA-damage signal. These observations allude to a separate mechanism by which telomerase inhibition could affect telomere-maintenance kinetics and homeostasis. Our data

505 is relevant for understanding the role of telomerase in the formation of higher-
506 order telomeric-chromatin structures and cell cycle progression, thereby
507 presenting new testable hypotheses and possibilities for combination drug
508 regimens.
509

510 **MATERIALS AND METHODS**

511 **Cell lines and reagents**

512 MCF-7, MDA-MB 231, HT29, LS180, BJ fibroblasts, and WI-38 VA-13
513 were obtained from the American Type Culture Collection (ATCC). MDA-MB 231
514 (NucLight Red) cells were obtained from Essen Bioscience. Cell culture media,
515 antibiotics, and other cell culture reagents were purchased from Invitrogen/Life
516 Technologies unless otherwise noted. Cells were maintained under standard
517 culture conditions of 37°C and 5% CO_2 with penicillin and streptomycin antibiotics
518 (100 U each) and in the presence of appropriate fetal bovine serum (FBS)
519 concentrations (5-15%), as indicated by the ATCC.

520 Etoposide (Sigma/Aldrich) was administered in dose-response treatments
521 in 2-fold serial dilution and a maximum dose of 10uM. ATM inhibitor KU55933
522 (Calbiochem) was administered as 10 μM in DMSO, a concentration previously
523 determined to efficiently inhibit ATM function (5,21,25). Imetelstat and its
524 mismatch oligo control (MM) were obtained from Geron, resuspended in PBS,
525 and stored at -20°C. Stock concentrations were determined before each
526 experiment using UV-spectrophotometer absorbance. Imetelstat and MM were

527 administered at 10 μM, a dose previously determined to inhibit telomerase
528 activity by >100 fold in multiple cancer cell types (5).
529
530 **Colony forming unit assay (CFU)**
531 The assay was performed as previously described (1,5). Cells were seeded and
532 allowed to grow into individual colonies at 37°C under 5% CO_2 for 2 weeks.
533 Colonies were counted as positive if colony sizes exceeded 50 μm. Dose-
534 response analysis was performed using GraphPad Prism (v6.0b).
535
536 **Immunocytochemistry (ICC)**
537 Labeling was conducted as previously described (5,23,24). Primary antibodies
538 were sourced and diluted as follows: anti-phospho-histone H2AX (Ser139) 1:500
539 (JBW301 EMD Millipore), phospho-H3 1:500 (06-570 EMD Millipore), and cyclin
540 B1 1:100 (Santa Cruz H-433). Images were collected using a Zeiss LSM 700
541 confocal microscope and Zen 2012 (Zeiss) software. To quantify DNA-damage
542 response foci, the collected images were blinded and scored with >400 cells
543 analyzed for each condition. Nuclear abnormality scoring was conducted as
544 previously described (39).
545
546 **Fluorescence-activated cell sorting (FACS)**
547 Cells were plated and allowed to settle before treatment for 24 to 48 h with the
548 described drug regimens. The treated cells were harvested by trypsinization and
549 fixed with ethanol. FITC-Anti-Cyclin B1 (BD Biosciences) immunolabeling and

propidium iodide nucleic acid labeling were conducted according to the manufacturer's protocol (Becton Dickinson). RNAse treatment was used to remove non-specific signals. Labeled cells were sorted using a BD LSRII flow cytometer (UBC Life Sciences Institute). For each cell sample, a minimum of 10,000 events were recorded. Flow Jo (Tree Star Inc) software and standard gating procedures were used to quantify the sub-G1 population and the number of cells with 2N and 4N DNA content.

Chromatin-immunoprecipitation (ChIP)

Cells were plated in 10 cm plates and allowed to settle before treatment for 24 h with the described drug regimens. The treated cells were PBS-washed and cross-linked in 1% formaldehyde. Cross-linked samples were collected by scraping in ChIP lysis buffer (20 mM Tris-HCl pH 8.0, 140 mM NaCl, 1 mM EDTA pH 8.0, 1% Triton X-100, 0.1% SDS, 1X protease inhibitor cocktail) and sonicated with a Covaris m220 ultrasonicator. The sonicated fractions were then precleared with Protein G sepharose beads (GE Healthcare, #17-0618) and then subjected to immunoprecipitation (IP) with 3 µg of anti-phospho-Histone H2A.X (Millipore 05-636). IP with 30 µL of BSA-preblocked protein G beads (without primary antibody) was used as control. Chromatin immunoprecipitates were washed sequentially in ChIP Wash Buffer A (0.1% SDS, 1% Triton X-100, 2 mM EDTA, 20 mM Tris-HCl pH 8.0, 150 mM NaCl), ChIP Wash Buffer B (0.1% SDS, 1% Triton X-100, 2 mM EDTA, 20 mM Tris-HCl pH 8.0, 500 mM NaCl), ChIP Wash Buffer C (0.25 M LiCl, 1% NP-40, 1% Sodium Deoxycholate, 1 mM EDTA,

10 mM Tris-HCl pH 8.0), and lastly TE buffer. The ChIP samples were reversed cross-linked overnight in 65°C, and extracted DNA was purified with a DNA cleanup kit (BioBasic). Quantitative PCR was performed using a Tel1b (telomere sequence) primer set (Forward: CGGTTTGTTTGGGTTTGGGTTTGGGTTTGGGTTTGGGTT, Reverse: GGCTTGCCTTACCCTTACCCTTACCCTTACCCTTACCCT) and an Alu repeat reference primer set (Forward: GACCATCCCGGCTAAAACG, Reverse: CGGGTTCACGCCATTCTC) (40).

Data analysis

GraphPad Prism version 6 (GraphPad Software Inc, San Diego, CA) was used for statistical analysis and data presentation. Student's *t*-tests or, where appropriate, ANOVA followed by Fisher's LSD test were used to generate P-values. $P < 0.05$ was considered statistically significant.

ACKNOWLEDGEMENTS

We thank Geron Corporation for the gift of imetelstat. We appreciate assistance from Arthur Chen for quantifying the ICC images, Andy Johnson for FACS use and analysis, and JiaLin Xu for technical help with TRAP experiments. Anna Krassowska, Neeru Batra from Geron, and members of the Wong Lab are thanked for critically reading the manuscript.

596 **REFERENCES**
597
598 1. Shay JW. Role of Telomeres and Telomerase in Aging and Cancer.
599 Cancer Discov. 2016 Jun;6(6):584–93.

600 2. Hukezalie KR, Wong JM. Structure-Function Relationship and Biogenesis
601 Regulation of the Human Telomerase Holoenzyme. FEBS J. 2013 Apr 3.

602 3. Shay JW, Wright WE. Hayflick, his limit, and cellular ageing. Nat. Rev. Mol.
603 Cell Biol. 2000 Oct;1(1):72-6.

604 4. Shay JW, Wright WE. Role of telomeres and telomerase in cancer. Semin.
605 Cancer Biol. 2011 Dec;21(6):349–53.

606 5. Tamakawa RA, Fleisig HB, Wong JMY. Telomerase inhibition potentiates
607 the effects of genotoxic agents in breast and colorectal cancer cells in a
608 cell cycle-specific manner. Cancer Res. 2010 Nov 1;70(21):8684–94.

609 6. Martínez P, Blasco MA. Telomeric and extra-telomeric roles for telomerase
610 and the telomere-binding proteins. Nat. Rev. Cancer. 2011 Mar;11(3):161–
611 76.

612 7. Giraud-Panis M-J, Pisano S, Benarroch-Popivker D, Pei B, Le Du M-H,
613 Gilson E. One identity or more for telomeres? Front Oncol. 2013;3:48.

614 8. Wong JMY, Collins K. Telomere maintenance and disease. Lancet. 2003
615 Sep 20;362(9388):983–8.

616 9. Shay JW, Bacchetti S. A survey of telomerase activity in human cancer.
617 Eur. J. Cancer. 1997 Apr;33(5):787–91.

618 10. Lenain C, Bauwens S, Amiard S, Brunori M, Giraud-Panis M-J, Gilson E.
619 The Apollo 5' exonuclease functions together with TRF2 to protect
620 telomeres from DNA repair. Curr. Biol. 2006 Jul 11;16(13):1303–10.

621 11. García-Cao M, O'Sullivan R, Peters AHFM, Jenuwein T, Blasco MA.
622 Epigenetic regulation of telomere length in mammalian cells by the
623 Suv39h1 and Suv39h2 histone methyltransferases. Nat. Genet. 2004
624 Jan;36(1):94–9.

625 12. Arnoult N, Karlseder J. Complex interactions between the DNA-damage
626 response and mammalian telomeres. Nat. Struct. Mol. Biol. 2015
627 Nov;22(11):859–66.

628 13. Collins K. The biogenesis and regulation of telomerase holoenzymes. Nat.
629 Rev. Mol. Cell Biol. 2006 Jul;7(7):484–94.

630 14. Chan SS, Chang S. Defending the end zone: studying the players involved

in protecting chromosome ends. FEBS Lett. 2010 Sep 10;584(17):3773–8.

15. Wu P, Takai H, de Lange T. Telomeric 3' overhangs derive from resection by Exo1 and Apollo and fill-in by POT1b-associated CST. Cell. 2012 Jul 6;150(1):39–52.

16. Martínez P, Blasco MA. Replicating through telomeres: a means to an end. Trends Biochem. Sci. 2015 Sep;40(9):504–15.

17. Zhong FL, Batista LFZ, Freund A, Pech MF, Venteicher AS, Artandi SE. TPP1 OB-fold domain controls telomere maintenance by recruiting telomerase to chromosome ends. Cell. 2012 Aug 3;150(3):481–94.

18. Nandakumar J, Cech TR. Finding the end: recruitment of telomerase to telomeres. Nat. Rev. Mol. Cell Biol. 2013 Feb;14(2):69–82.

19. Kibe T, Zimmermann M, de Lange T. TPP1 Blocks an ATR-Mediated Resection Mechanism at Telomeres. Mol. Cell. 2016 Jan 21;61(2):236–46.

20. Herbert B-S, Gellert GC, Hochreiter A, Pongracz K, Wright WE, Zielinska D, et al. Lipid modification of GRN163, an N3“-->P5” thio-phosphoramidate oligonucleotide, enhances the potency of telomerase inhibition. Oncogene. 2005 Aug 4;24(33):5262–8.

21. Verdun RE, Karlseder J. The DNA damage machinery and homologous recombination pathway act consecutively to protect human telomeres. Cell. 2006 Nov 17;127(4):709–20.

22. Tong AS, Stern JL, Sfeir A, Kartawinata M, de Lange T, Zhu X-D, et al. ATM and ATR Signaling Regulate the Recruitment of Human Telomerase to Telomeres. Cell Rep. 2015 Nov 24;13(8):1633–46.

23. Tefferi A, Lasho TL, Begna KH, Patnaik MM, Zblewski DL, Finke CM, et al. A Pilot Study of the Telomerase Inhibitor Imetelstat for Myelofibrosis. N. Engl. J. Med. 2015 Sep 3;373(10):908–19.

24. Jafri MA, Ansari SA, Alqahtani MH, Shay JW. Roles of telomeres and telomerase in cancer, and advances in telomerase-targeted therapies. Genome Med. 2016;8(1):69.

25. Verdun RE, Crabbe L, Haggblom C, Karlseder J. Functional human telomeres are recognized as DNA damage in G2 of the cell cycle. Mol. Cell. 2005 Nov 23;20(4):551–61.

26. Takai H, Smogorzewska A, de Lange T. DNA damage foci at dysfunctional telomeres. Curr. Biol. 2003 Sep 2;13(17):1549–56.

27. Asai A, Oshima Y, Yamamoto Y, Uochi TA, Kusaka H, Akinaga S,

Yamashita Y, Pongracz K, Pruzan R, Wunder E, Piatyszek M, Li S, Chin AC, Harley CB, Gryaznov S. A novel telomerase template antagonist (GRN163) as a potential anticancer agent. Cancer Res 2003 Jul 15;63(14):3931–9.

28. Bryan TM, Englezou A, Dalla-Pozza L, Dunham MA, Reddel RR. Evidence for an alternative mechanism for maintaining telomere length in human tumors and tumor-derived cell lines. Nat. Med. 1997 Nov;3(11):1271–4.),

29. Fleisig HB, Wong JMY. Telomerase promotes efficient cell cycle kinetics and confers growth advantage to telomerase-negative transformed human cells. Oncogene. 2012 Feb 23;31(8):954–65.

30. Shiloh Y, Ziv Y. The ATM protein kinase: regulating the cellular response to genotoxic stress, and more. Nat. Rev. Mol. Cell Biol. 2013 Apr;14(4):197-210.

31. Bolderson E, Tomimatsu N, Richard DJ, Boucher D, Kumar R, Pandita TK, et al. Phosphorylation of Exo1 modulates homologous recombination repair of DNA double-strand breaks. Nucleic Acids Res. 2010 Apr;38(6):1821–31.

32. Xie Z, Jay KA, Smith DL, Zhang Y, Liu Z, Zheng J, et al. Early telomerase inactivation accelerates aging independently of telomere length. Cell. 2015 Feb 26;160(5):928–39.

33. Burgess DJ, Doles J, Zender L, Xue W, Ma B, McCombie WR, et al. Topoisomerase levels determine chemotherapy response in vitro and in vivo. Proc. Natl. Acad. Sci. U.S.A. 2008 Jul 1;105(26):9053–8.

34. Lee SS, Bohrson C, Pike AM, Wheelan SJ, Greider CW. ATM Kinase Is Required for Telomere Elongation in Mouse and Human Cells. Cell Rep. 2015 Nov 24;13(8):1623–32.

35. Blasina A, Price BD, Turenne GA, McGowan CH. Caffeine inhibits the checkpoint kinase ATM. Curr. Biol. 1999 Oct 7;9(19):1135-8.

36. Shibata A, Barton O, Noon AT, Dahm K, Deckbar D, Goodarzi AA, et al. Role of ATM and the damage response mediator proteins 53BP1 and MDC1 in the maintenance of G(2)/M checkpoint arrest. Mol. Cell. Biol. 2010 Jul;30(13):3371–83.

37. Baerlocher GM, Oppliger Leibundgut E, Ottmann OG, Spitzer G, Odenike O, McDevitt MA, et al. Telomerase Inhibitor Imetelstat in Patients with Essential Thrombocythemia. N. Engl. J. Med. 2015 Sep 3;373(10):920–8.

38. Kohnken R, Kodigepalli KM, Wu L. Regulation of deoxynucleotide metabolism in cancer: novel mechanisms and therapeutic implications. Mol. Cancer. 2015;14:176.

703 39. Fleisig HB, Hukezalie KR, Thompson CAH, Au-Yeung TTT, Ludlow AT,
704 Zhao CR, et al. Telomerase reverse transcriptase expression protects
705 transformed human cells against DNA-damaging agents, and increases
706 tolerance to chromosomal instability. Oncogene. 2016 Jan 14;35(2):218–
707 27.

708 40. Keefe D, Wang F, Robinson LG, Pan XV, Weissman SM, Liu L, Kalmbach
709 KH. Measurement of telomere length at the single cell level. Protoc. Exch.
710 2017 Jan 5.

711

712

713
714
715
716
717

FIGURES

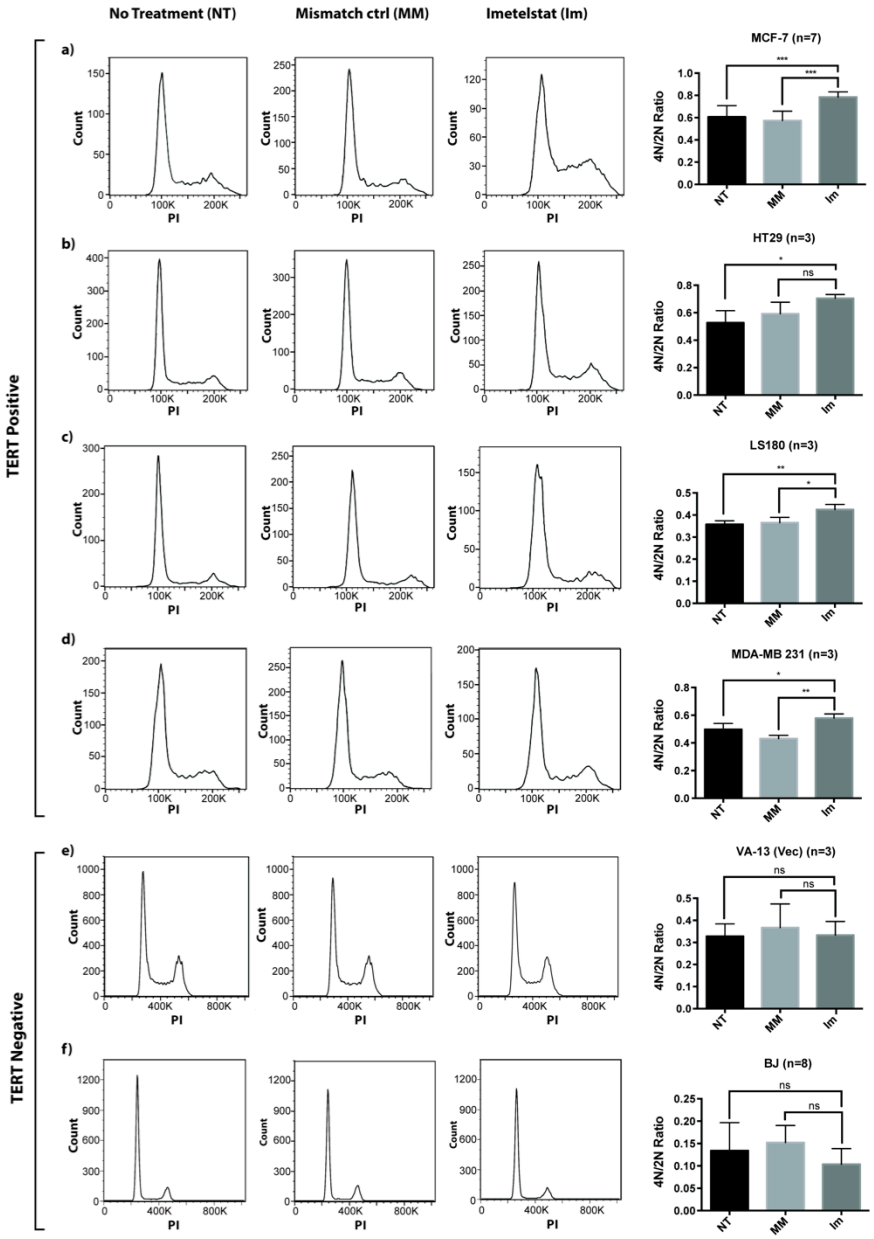

Figure 1. Telomerase inhibition increases the proportion of telomerase-positive cells with 4N DNA content. Cells were treated for 24 h with 10 μM imetelstat (Im) or its mismatch oligo control (MM). DNA content was analyzed using FACS and gating single cells by propidium iodide (PI) staining. Representative cell cycle profiles are shown for the indicated treatments and cell lines. (a-d) Imetelstat-induced telomerase inhibition increased the ratio of 4N to 2N cells in MCF-7, HT29, LS180, and MDA-MB 231 cell lines. (e-f) No change in ratio was observed in telomerase-negative VA-13 and BJ cell lines. ANOVA and Fisher's LSD test were used to generate P-values (* = P ≤0.05, ** = P ≤ 0.01, *** = P ≤ 0.001). Error bars represent SD.

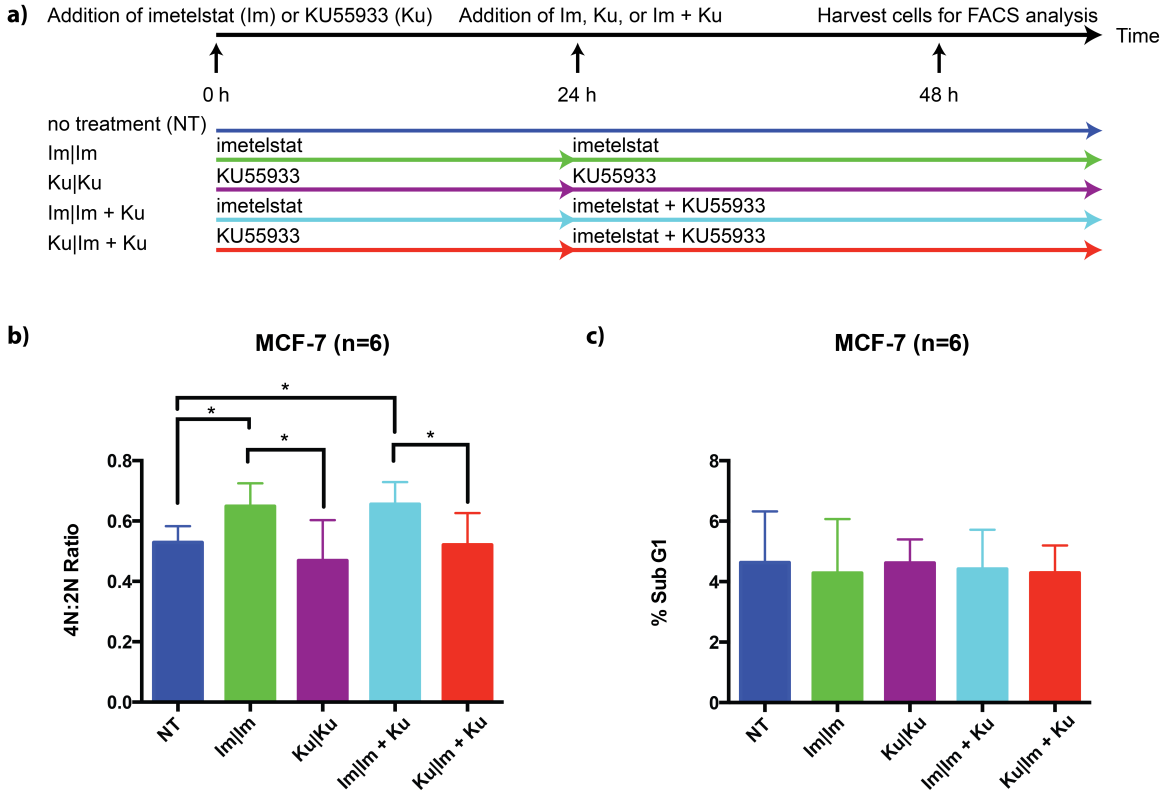

Figure 2. KU55933 and imetelstat affects cell cycle population distribution. (a) MCF-7 cells were treated with the indicated inhibitors (first 24 h | second 24 h) for 48 h. FACS analysis with propidium iodide staining was used to determine the 4N to 2N ratio. (b) Imetelstat (Im|Im) and imetelstat in combination with KU55933 (Im|Im + K) increased 4N DNA cell populations compared to no treatment (NT). Treatment with KU55933 in the first 24 h decreased 4N DNA cell populations compared to the respective treatment regimens using imetelstat in the first 24 h. (c) No difference in sub-G1 populations, a readout of apoptosis and cell death, was observed among cell lines undergoing different treatment regimens. ANOVA and Fisher's LSD test were used to generate P-values (* = P ≤0.05). Error bars represent SD.

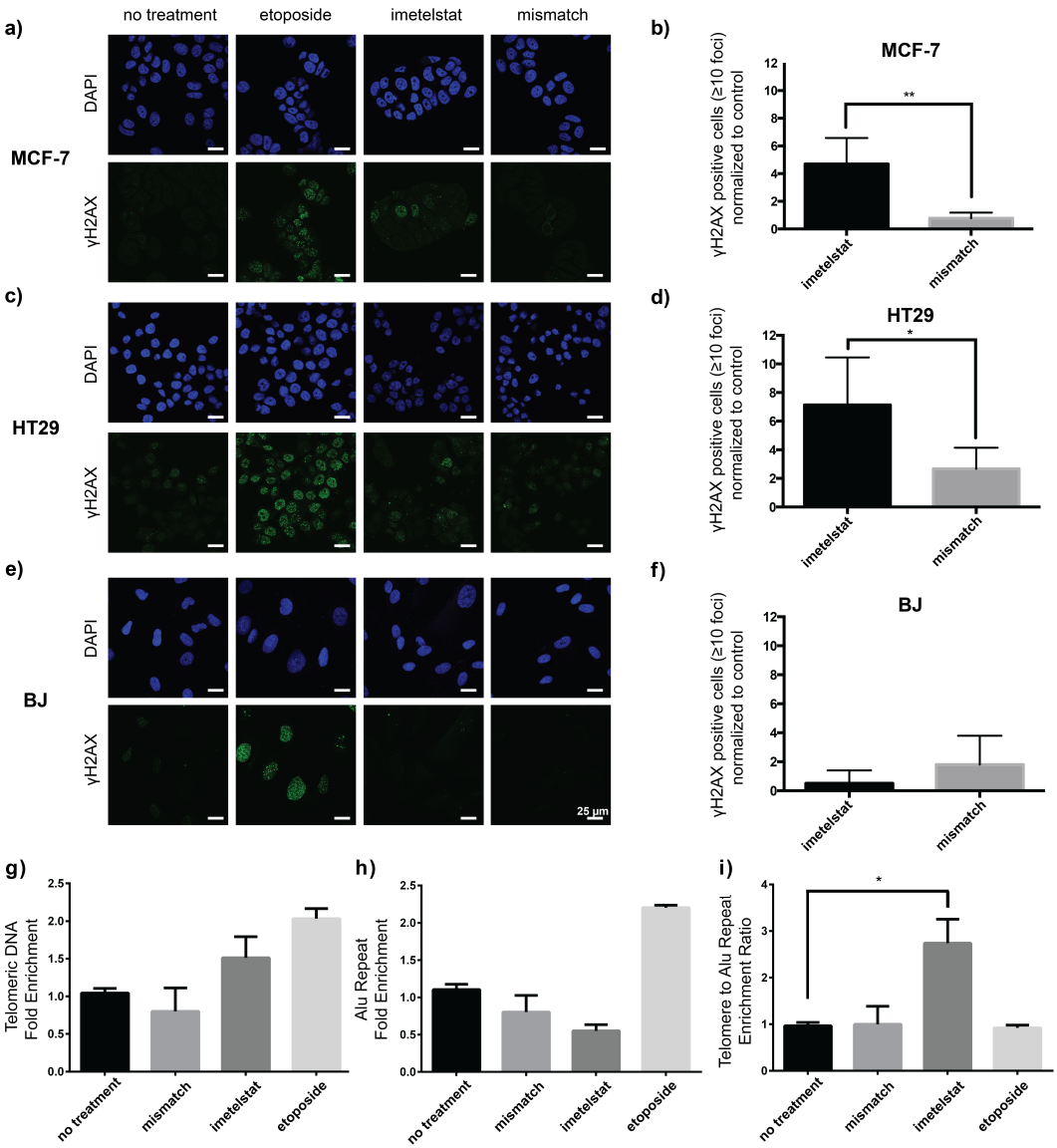

Figure 3. Telomerase inhibition induces DNA damage foci in telomerase-positive but not telomerase-negative cells. (a-d) Immunocytochemistry showed increased γH2AX DNA damage foci in a subset of telomerase-positive MCF-7 and HT29 cells treated for 24 h with imetelstat (10 μM). The mismatch control oligo (10 μM) did not induce this effect. Etoposide (1.4 μM) was used as a positive control. (e-f) Imetelstat did not induce DNA damage foci in telomerase-negative BJ primary human fibroblasts. Histograms show accumulation of cells with ≥10 foci, normalized to the numbers obtained from no treatment controls. Error bars represent SD. (g-i) γH2AX-ChIP-qPCR of (g) telomeric region and (h) Alu repeat region in MCF-7 cells. Enrichment values were normalized to beads only controls. (i) The ratio of ChIP enrichment of telomeric region over the Alu reference regions was indicative of telomere-specific enrichment of γH2AX signals (i). Error bars represent SEM. Student's *t*-test was used to generate P-values (* = P ≤0.05, ** = P ≤ 0.01, n ≥ 3).

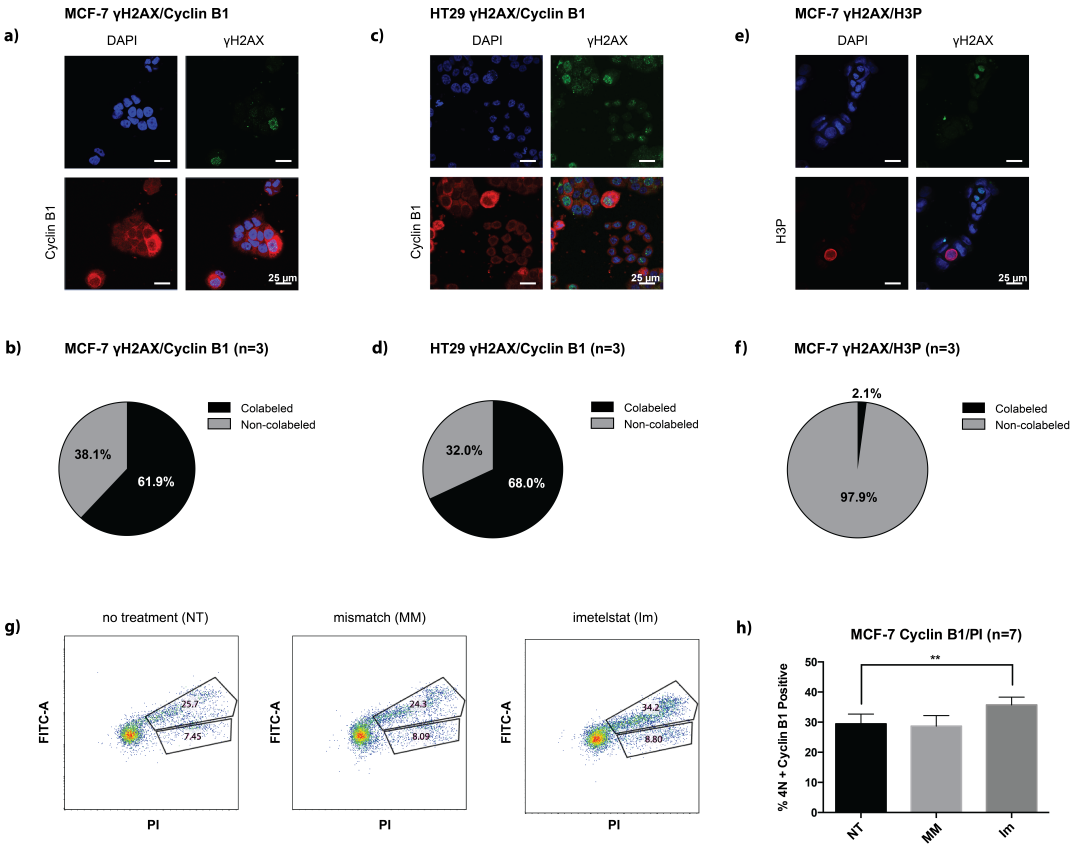

Figure 4. Imetelstat increases the population of cells in late S/G2 phases. (a-c) Following 24 h treatment with imetelstat (10 μM), MCF-7 and HT29 cells were labeled for γH2AX in combination with cytoplasmic cyclin B1, a marker of late S/G2 phases, or phospho-histone H3 (H3P), a marker of M phase. (d-f) DNA damage foci-positive cells (≥10 foci) co-labeled with cyclin B1 or H3P were quantified, with >400 cells analyzed for each condition. (g-h) MCF-7 cells were treated with imetelstat (Im), the mismatch oligo (MM) or no drug (NT) for 24 h then labeled with FITC-conjugated anti-cyclin B1 and propidium iodide (PI). ANOVA and Fisher's LSD test were used to generate P-values (* = P ≤0.05, ** = P ≤ 0.01). Error bars represent SD.

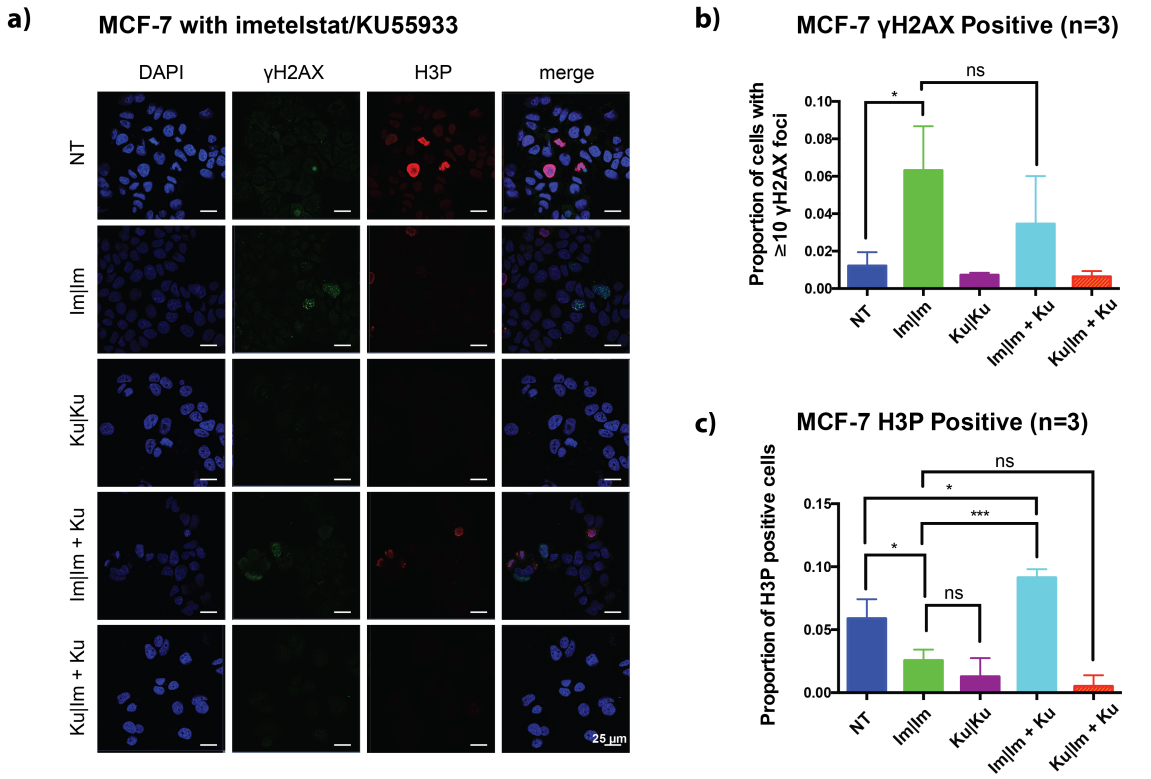

Figure 5. Functional ATM signaling is required for imetelstat-induced DNA damage foci formation and the G2/M checkpoint stall. (a) MCF-7 cells were treated with the indicated inhibitor(s) for 48 h using the same scheme as Fig. 2 before γH2AX and phospho-histone H3 (H3P) labeling. (b-c) Images were scored blindly to quantify co-labeling, with >400 cells scored per condition. ANOVA and Fisher's LSD test were used to generate P-values (* = P ≤0.05, ** = P ≤ 0.01, *** = P ≤ 0.001). Error bars represent SD.

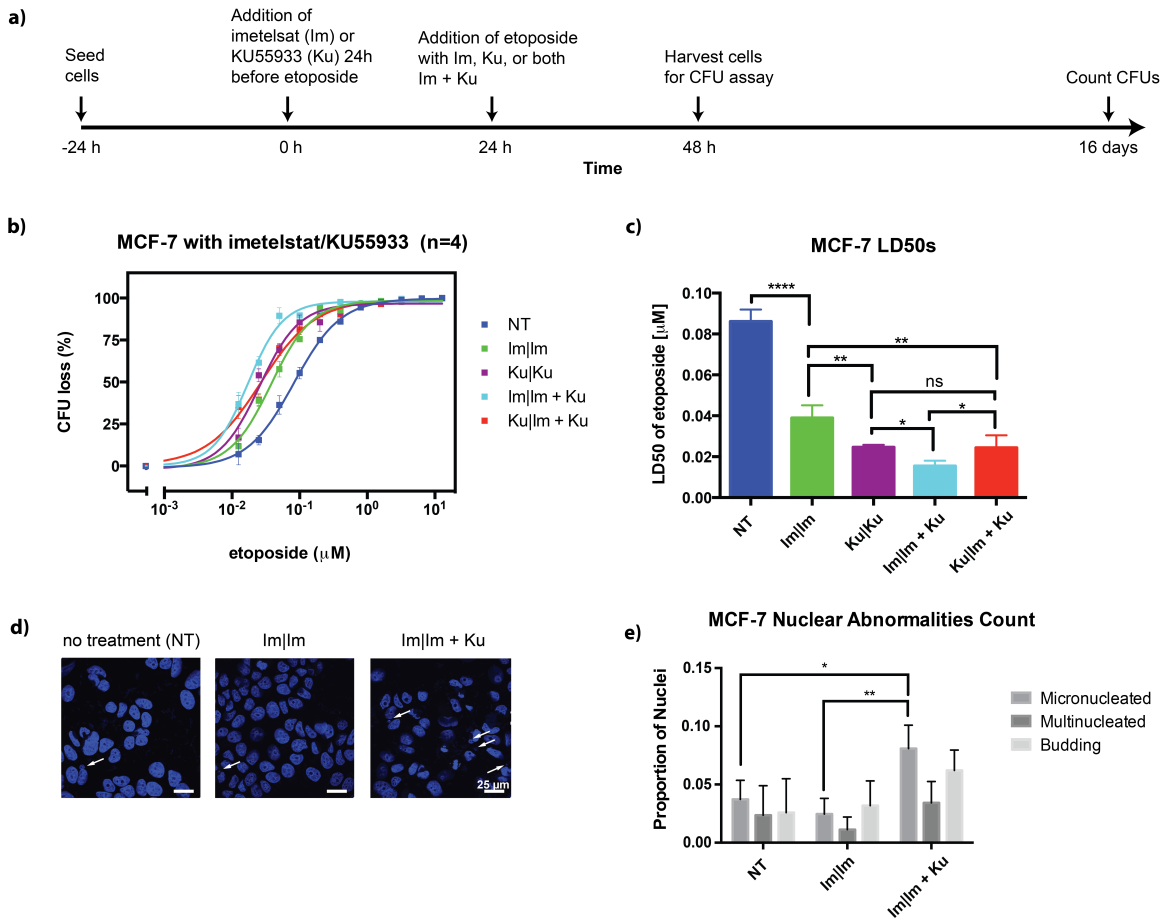

Figure 6. Imetelstat potentiation of etoposide cytotoxicity requires functional ATM signaling. (a) MCF-7 cells were treated with imetelstat (10 μM) or KU55933 (10 μM) for 24 h prior to addition of serial dilutions of etoposide (12.8 – 0.0125 μM) in combination with the previously used inhibitor or in combination with both inhibitors (Im + Ku). After 24 h incubation with etoposide, cells were counted and seeded in soft agar using the colony formation assay (CFU). Colonies were scored after 14 days. (b) Dose-response curves of MCF-7 cells given the indicated inhibitors (first 24 h | second 24 h in combination with etoposide) or no treatment (NT) before etoposide addition. (c) LD_{50}s obtained from dose-response curves. Error bars represent SEM. (d) Representative images of DAPI nuclear staining for treatments examined. Arrows indicate micronuclei. (e) Nuclear abnormalities were quantified from the same sets of images as in Fig. 5. Error bars represent SD. ANOVA and Fisher's LSD test were used to generate P-values (* = P ≤0.05, ** = P ≤ 0.01, *** = P ≤ 0.001, **** = P ≤ 0.0001).